CMS Physics Analysis Summary

Contact: cms-pog-conveners-jetmet@cern.ch 2014/08/23

Study of Pileup Removal Algorithms for Jets

The CMS Collaboration

Abstract

One of the main challenges of the upcoming LHC run will be the increase of instantaneous luminosity, which will result in a large number of additional proton-proton collisions in each event (pileup). In such a high pileup environment, the accurate reconstruction of jet properties and shapes will be more and more demanding. In this note, the performances of various advanced pileup mitigation tools such as charged hadron subtraction, grooming techniques, jet cleansing and per particle pileup approaches are studied. The focus is on preparation for LHC Run II for which we expect up to 40 additional pileup events on average and includes comparisons to LHC Run I data which has typically 20 additional pileup events on average.

Contents

1 Introduction 2
2 CMS detector and event reconstruction 3
3 Datasets and simulated samples 3
4 Charged hadron subtraction 4
4.1 Physics objects and event selection 5
4.2 MC based study 5
4.3 Data-MC comparisons 9
5 Grooming algorithms 9
5.1 Physics objects and event selection 11
5.2 Higher pileup studies for LHC Run II 11
5.3 Data-MC comparisons from LHC Run I 17
6 Pileup mitigation tools 18
6.1 Physics objects and event selection 19
6.2 Higher pileup studies for LHC Run II 19
6.3 Data-MC comparisons from LHC Run I 24
7 Conclusions 27

1 Introduction

The performance of jets is extremely important to the success of physics at the LHC in both measurements and searches. One of the outstanding challenges of the upcoming LHC run will be the increase of instantaneous luminosity, which will result in a large number of additional proton-proton collisions in each event (pileup). In such a high pileup environment, the accurate reconstruction of jet properties and shapes will become more and more demanding. The most common observables for jets at the LHC consider the jet as a 4-vector and are primarily the jet p_{T}, η, and ϕ. In recent years, it has become increasingly popular to consider the internal structure of the jet. The applications include the discrimination of quark- and gluon-initiated jets [1] as well as the identification of highly boosted heavy resonances [2, 3], for which all decay products are reconstructed within a single jet.

In all such cases, contamination to the jet from pileup degrades the ability to reconstruct the jet observables. Within this study, we examine advanced techniques for pileup mitigation in jets in view of high pileup scenarios expected in Run II of the LHC where the typical event contains 40 additional pileup events on average compared to the typical 20 pileup events experienced during LHC Run I. At CMS [4], multiple techniques for mitigating the effects of pileup are exploited. The baseline method for correcting the jet for pileup is to apply an offset to the jet energy. The method is described in more detail in [5]. This technique requires the estimation of the average amount of transverse energy in the event per unit area coming from pileup, which is typically called ρ. A portion of this transverse energy, dependent on the jet area [6], p_{T} and η, is subtracted from the jet energy as a correction.

While this technique has been shown to be successful in Run I, further improvements are possible. The transverse energy correction only corrects the jet four-vector, but does not make a correction to jet structure observables. Furthermore, there are additional handles against pileup at CMS. The first is the use of tracking information which takes advantage of the fact that a large fraction of the pileup vertices are separated in space from the vertex of interest. Therefore, charged particles from pileup vertices can be removed from the jets, in a process called "charged hadron subtraction" (CHS). The performance of CHS jets will be discussed in Section 4.

Additionally, we can use the local shape of the radiation to help us identify contributions to the jet from pileup. The technique of jet grooming was originally intended to remove soft and collinear radiation from the jet. The primary use was for reducing the effect of this radiation on the jet mass in order to identify jets produced from heavy resonance decays. However, it can also be used to mitigate the effect of pileup on the jet as well. There are many different types of jet grooming algorithms including trimming [7], pruning [8], soft drop [9] and modified mass drop tagger [10]. These are the grooming algorithms considered in this note. The basic idea is the same in all cases: they aim to identify the hard structure in the jet and "groom" away the softer components. In Section 5, we examine and compare the performance of different grooming algorithms and different parameters within these grooming algorithms.

Finally, in Section 6 we examine more advanced methods which can take advantage of the multiple handles for the pileup mitigation. There are several new methods proposed for pileup mitigation including constituent subtraction [11], jet cleansing [12], and pileup per particle identification (PUPPI) [13]. In these cases, we examine the performance of these advanced algorithms, both in terms of jet p_{T} reconstruction and jet shapes, and compare their performance to the methods above.

2 CMS detector and event reconstruction

A detailed description of the CMS detector can be found in [4].

The central feature of the CMS detector is a 3.8 T superconducting solenoid of 6 m internal diameter. Within the field volume are the silicon tracker, the crystal electromagnetic calorimeter (ECAL), and the brass-scintillator hadron calorimeter (HCAL). The muon system is installed outside the solenoid and embedded in the steel return yoke. CMS uses a right-handed coordinate system, with the origin at the nominal interaction point, the z axis pointing along the direction of the counter-clockwise beam, the y axis pointing up (perpendicular to the LHC plane), and the x axis chosen to make a right-handed coordinate system. The polar angle θ is measured from the positive z axis, the azimuthal angle ϕ is measured in the $x - y$ plane and the pseudorapidity is defined as $\eta \equiv -\ln[\tan(\theta/2)]$.

The CMS tracker consists of 1440 silicon pixel and 15 148 silicon strip detector modules, with full azimuthal coverage within η <2.5. The ECAL consists of 75 848 lead tungstate crystals, which provide coverage in pseudorapidity $|\eta| < 1.479$ in the central barrel region and $1.479 < |\eta| < 3.0$ in the two forward endcap regions. The HCAL is a sampling calorimeter which utilizes alternating layers of brass or steel as absorber and plastic scintillator as active material. The muon system includes barrel drift tubes covering the pseudorapidity range $|\eta| < 1.2$, endcap cathode strip chambers ($0.9 < |\eta| < 2.5$), and resistive plate chambers ($|\eta| < 1.6$).

Jets are reconstructed by clustering the set of objects obtained by the particle flow algorithm [14, 15] (PF candidates). The particle flow technique reconstructs and identifies each single particle with an optimized combination of all subdetector information. The energy of photons is obtained directly from the ECAL measurement, corrected for zero-suppression effects. The energy of electrons is determined from a combination of the track momentum at the main interaction vertex, the corresponding ECAL cluster energy, and the energy sum of all bremsstrahlung photons attached to the track. The energy of muons is obtained from the corresponding track momentum. The energy of charged hadrons is determined from a combination of the track momentum and the corresponding ECAL and HCAL energy, corrected for zero-suppression effects, and calibrated for the nonlinear response of the calorimeters. Finally, the energy of neutral hadrons is obtained from the corresponding calibrated ECAL and HCAL energy. The primary interaction vertex is defined as the vertex with the highest sum of the squared transverse momenta of the charged tracks associated to it.

In order to make comparisons with reconstructed jets, we often compare to the simulation at particle level before any detector reconstruction. These particle inputs exist only for the hard scatter and do not include pileup particles. Particle level jets are clustered from simulated final state particles after parton showering, hadronization, and the decay of hadrons with lifetimes too short to interact with the detector, excluding particles invisible to the detector such as neutrinos.

3 Datasets and simulated samples

This study considers data recorded with the CMS detector during the year 2012, at a center of mass energy $\sqrt{s} = 8$ TeV.

Two topologies are considered for the analysis: dijets and photon (γ) + jets. The dijet topology is used to get a large sample of high p_{T} jets that can be used particularly in the study of jet substructure observables. The γ + jets channel is used in studies of CHS in order to define jets from the hard scatter recoiling off of the photon.

For studies with data, the dijet sample is collected using the logical "or" of a set of triggers based on requirements on $H_T = \sum_{jets} p_T$ (here p_T is the transverse momentum of a jet) with the sum running over jets with $p_T > 40$ GeV, and the dijet invariant mass of the two highest p_T jets in an event. The event selection follows closely the resonance search in Ref [16]. Events are initially selected by requiring at least two jets with $p_T > 30$ GeV and $|\eta| < 2.4$. The two highest-p_T jets are required to have a pseudorapidity separation $|\Delta\eta| < 1.3$, which rejects a large fraction of QCD multijet background in view of a resonance search. Finally, the dijet invariant mass is required to be larger than 890 GeV. This threshold is defined by the trigger selection, which was found to be 99% efficient for events with dijet masses above this threshold. W-tagging is studied using the leading jet in the selected dijet events with additional requirements on the jet p_T. For low p_T studies of CHS performance, the γ + jets topology is also considered. The considered events were recorded with triggers requiring one photon with variable p_T thresholds and selection criteria, depending on the running period.

The simulated samples can be broadly classified into two main scenarios corresponding to the LHC conditions of 2012 (Run I) and one expected set of LHC parameters for 2015 (Run II) with more pileup than in 2012. The Run I scenario roughly corresponds to the data sample collected in 2012 at $\sqrt{s} = 8$ TeV with an average amount of approximately 20 pileup interactions and a bunch spacing of 50 ns. This sample is used for data to simulation comparisons. The Run II scenario samples are simulated at $\sqrt{s} = 13$ TeV, with an average amount of pileup of 40 additional interactions per event and a bunch spacing of 50 ns.

The simulation processes considered are γ+jets and QCD multijets. In addition, a sample of Randall-Sundrum (RS) gravitons [17] with 1 TeV mass decaying to a pair of W bosons is used to study the performance of the different pileup mitigation tools on W jets in the high pileup scenario. The γ+jets sample and the corresponding QCD multijets background sample for the CHS analysis in the Run I scenario are simulated with PYTHIA 6 [18], using the PYTHIA tune Z2* [19]. The QCD multijets sample used in the comparison to Run I high p_T jets data is simulated with Herwig++ [20]. The QCD multijets sample and RS graviton sample for the Run II scenario are generated with PYTHIA8 [21] with Tune 4C.

All simulated samples include the effect of additional inelastic proton-proton interactions within the same bunch crossing ("in-time pileup") as well as additional contributions in the signal readout from the previous and next bunch crossings ("out-of-time pileup"). Run I simulated events are weighted in order to match the number of interactions per beam crossing measured in data, this procedure takes into account the luminosity sections and trigger paths effectively used in the analysis.

Jet energy corrections are applied data and MC to account for the non-linear response of the calorimeters and other instrumental effects. For the 13 TeV MC samples, jet energy corrections derived from the 8 TeV ones are used [22]; additionally, dedicated corrections are applied to the jets p_T on top of the 8 TeV corrections in order to account for residual differences. These corrections have been derived by studying the p_T response of the reconstructed jets matched to generator level jets in the 13 TeV MC samples as a function of the generator level p_T and η.

4 Charged hadron subtraction

Charged Hadron Subtraction (CHS) is a technique used to reduce the effect of "in-time pileup" on reconstructed physics objects. In this approach, charged hadrons unambiguously associated to pileup vertices are removed from the event and the remaining PF candidates are allowed to cluster to form jets. This method (PF+CHS in the following) compares with the default jet algo-

rithm (PF in the following) where pileup identification is not attempted and all PF candidates, whether they be from pileup or otherwise, are allowed to cluster.

Charged hadrons are identified in the PF algorithm as a track, possibly associated with ECAL and HCAL hits. Since the tracker volume extends to $|\eta| < 2.5$, this is where CHS is relevant. The leading primary vertex (PV) is chosen based on the magnitude of the sum of squares of the track transverse momenta ($\sum |p_{\mathrm{T}}^{\mathrm{TRK}}|^2$). Subleading PV's are classified as pileup vertices, and are required to pass further quality criteria based on a minimum number of degrees of freedom in the vertex fit, $N_{\mathrm{dof}} > 4$. Based on compatibility with reconstructed primary vertices, charged hadrons can be assigned to the chosen vertex, or pileup vertices. This designation is based on the chi-square per degree of freedom (χ^2/d.o.f.) of the track to a proto-vertex reconstructed without it. If χ^2/d.o.f. < 20 for a proto-vertex, then the track is associated to this (and only this) vertex. If the track from a charged hadron is associated to a good pileup PV, it is considered a pileup track, and removed in the CHS procedure. All other tracks, including those not associated to any PV, are kept.

In this section, we compare the performances of the PF+CHS procedure with respect to the standard PF on jet reconstruction, using events with one prompt photon and at least one jet. In both cases, jets are clustered using an anti-kT [23] algorithm with distance parameter $R = 0.5$, and their energy is corrected to account for residual pile-up and nonlinear calorimetric response, as a function of η and p_{T}. The applied corrections are different depending on whether CHS is applied.

4.1 Physics objects and event selection

The studies in this section are based on LHC Run I data and the corresponding simulation. Events considered in this analysis are required to contain exactly one photon, with $p_T > 85$ GeV and $|\eta| < 1.3$, and no isolated electron or muon. Photons are required to pass standard isolation and identification criteria, with a typical efficiency of 90%. This selection has a rejection rate of about 96% in the barrel for photons originating from hadrons in W+jet events [24].

In each event, jets with $p_{\mathrm{T}} > 20$ GeV are considered and two kinds of jets are distinguished. If they are close enough to the photon ($\Delta\phi(\gamma, \mathrm{jet}) < 1$), they are considered as belonging to the "pileup enriched area". On the contrary, if a jet and the photon are back to back ($\Delta\phi(\gamma, \mathrm{jet}) > 3$) and well balanced ($p_T(\mathrm{jet}) > 0.3 \cdot p_T(\gamma)$, and there is no other jet with $\Delta\phi(\gamma, \mathrm{jet}) > 3$, $p_T > 10$ GeV and $p_T > 0.2 \cdot p_T(\gamma)$ in the event), the jet is seen as coming from the "hard scattering" and the photon can be used as a probe of the "true" jet kinematic properties.

4.2 MC based study

In this section the performances of CHS are evaluated on a simulated sample of events containing one photon and one or more jets which follow the selection described in the previous section 4.1. Figure 1 (left) shows the p_T spectrum, for the two jet categories described above. Due to the photon momentum selection ($p_T^{\gamma} > 85$ GeV) and strict criteria on additional jets, the p_T for jets from the hard scattering process peaks around 90 GeV and there is at most one such jet per event. Jets from the pileup enriched area are typically softer, follow a decreasing p_T spectrum, and can be several per event. The CHS procedure changes the p_T spectrum of pileup jets and consequently also the multiplicity, as jets are requested to have $p_T > 20$ GeV. Most of the jets removed by CHS are soft ($p_T < 30$ GeV previous to CHS application).

The application of CHS removes a significant proportion of pileup energy from all jets, which improves the jet energy resolution at low p_T, as already seen in other studies with dijets [25]. In Fig. 1 (right), we see the ratio of reconstructed and generated jet p_T peaking more sharply

when CHS is applied. The effect of CHS is more pronounced for jets from the pileup enriched area at low p_T, where the relative impact of pileup offset energy is bigger. It should be noted, however, that the left-hand-side of the approximately Gaussian distribution is cut off due to the requirement on the reconstructed p_{T}, $p_{\mathrm{T,reco}} > 20$ GeV, because the generator level $p_{\mathrm{T,true}}$ peaks at low p_T for the pileup enriched area.

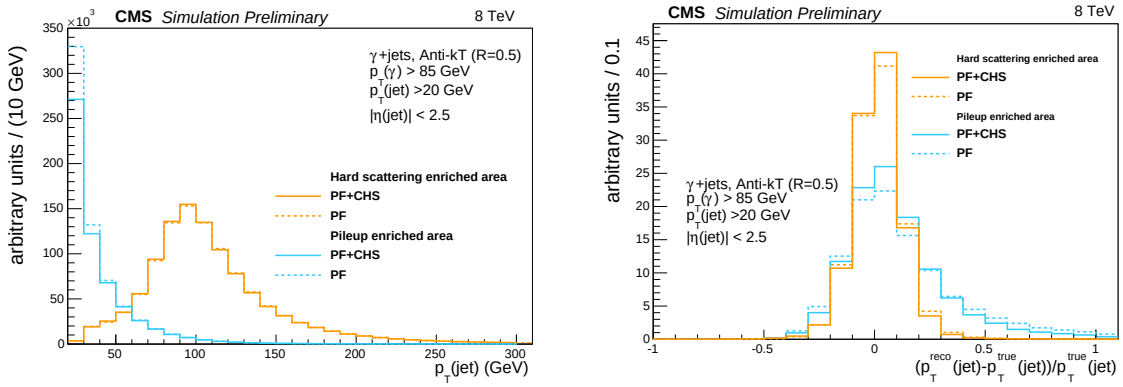

Figure 1: (Left) Transverse momentum distribution of jets from hard scatter and from pileup enriched area. Due to the tight selection, there can only be one or less than one jet from hard scattering. (Right) Ratio of reconstructed and true particle level jet p_T for PF and PF+CHS in the hard scatter and pileup enriched areas. The left-hand-side of an approximately Gaussian distribution is cut off by the $p_{\mathrm{T,reco}} > 20$ GeV requirement for $p_{\mathrm{T,true}}$ peaking at low p_T in the pileup enriched area.

The primary effect of CHS is the removal of jets from pileup. The signal and pileup jets can be identified in simulation by matching the reconstructed jets to jets clustered from generated hard scatter particles. The proper matching requires $\Delta R(\mathrm{gen,reco}) < 0.25$ between a particle level jet of $p_{\mathrm{T,gen}} > 10$ GeV and a reconstructed jet of $p_{\mathrm{T,reco}} > 20$ GeV. Unmatched jets typically have a high proportion of their energy from pileup interactions and are referred to as pileup jets. The matching efficiency is typically better than 99% for the jets from hard scatter, as seen in Fig. 2 (left). Of the jets in the pileup region, only about 80% are matched for the PF reconstruction, as expected from the higher proportion of pileup jets in this area. The application of CHS reduces the rate of unmatched pileup jets from 20% to approximately 5% in the tracker-covered region $|\eta| < 2.5$. The pileup jets are typically of low p_T, which explains the fraction of matched jets rising toward high p_T for both PF and PF+CHS, as seen in Fig. 2 (right).

In addition, we can look in more detail at the relative rates of PF and PF+CHS for matched jets from hard scatter and pileup enriched areas as well as the unmatched (pileup) jets from pileup enriched area. The results are shown in Fig. 3 as a function of η. The rates of matched jets are not appreciably changed by the application of CHS in either hard scatter or pileup enriched areas, whereas the rate of unmatched jets in the pileup enriched area drops by a factor three using CHS. There is no loss in the efficiency for matched jets while there is a great reduction in the pileup jet rate.

The application of CHS also improves the angular resolution of jets. This is demonstrated in Fig. 4, which shows the residual shifts in R between reconstructed and generated jets. Reconstructed jets are closer to the generated ones when CHS is applied. As expected, the effect is amplified for high levels of pileup as seen in Fig. 4 (right), where the RMS of the residual shifts in R between reconstructed and generated jets is shown as a function of the number of vertices.

As discussed, the charged hadron subtraction is possible only within the tracker acceptance and could hence generate some η bias for jets reconstructed on the tracker edges. In order to

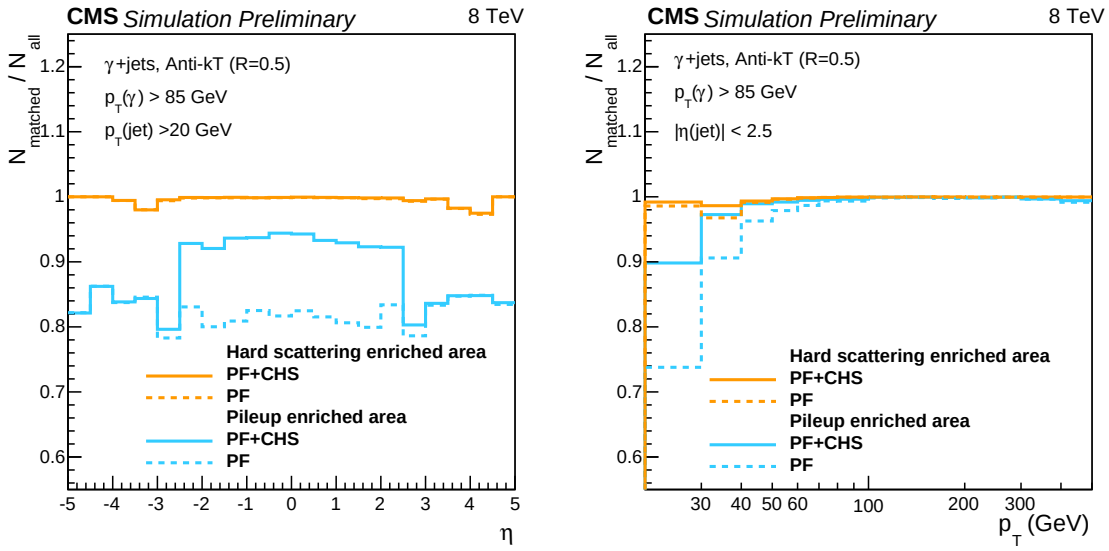

Figure 2: Ratio of reconstructed jets matched to particle level jets versus η (left) and p_T (right). The unmatched jets typically have a high proportion of their energy from pileup and are referred to as pileup jets. This plot demonstrates the reduction in pileup jet rate after applying CHS.

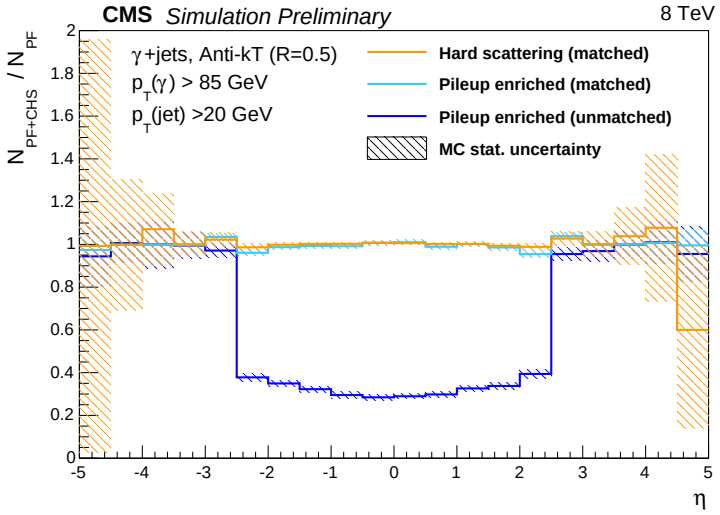

Figure 3: Ratio as a function of η of jet rates with PF and PF+CHS for matched jets from hard scatter, matched jets from pileup enriched area and unmatched jets from pileup enriched area. The matched jets are associated with good signal jets from hard scatter, while the unmatched ones are associated with pileup. The application of CHS reduces the pileup jet rate by factor three in the tracker-covered region $|\eta| < 2.5$. The hashed areas correspond to the MC statistical uncertainty.

check for possible migration of jets generated astride tracker edges that could be reconstructed above them, jets are categorized in several $(\eta^{\text{gen}}, p_T^{\text{gen}})$ bins and their relative shift in η is computed. Figure 5 shows the mean of the $(\eta^{\text{gen}} - \eta^{\text{reco}}) \cdot \text{sign}(\eta^{\text{gen}})$ distribution, as a function of η^{gen} and p_T^{gen}. While CHS seems to mitigate the bias in the central region, an induced bias is indeed observed around $|\eta| = 2.5$, where after CHS the jets are reconstructed with a value of $|\eta|$ which is bigger than the true one. This is consistent with the fact that the subtraction

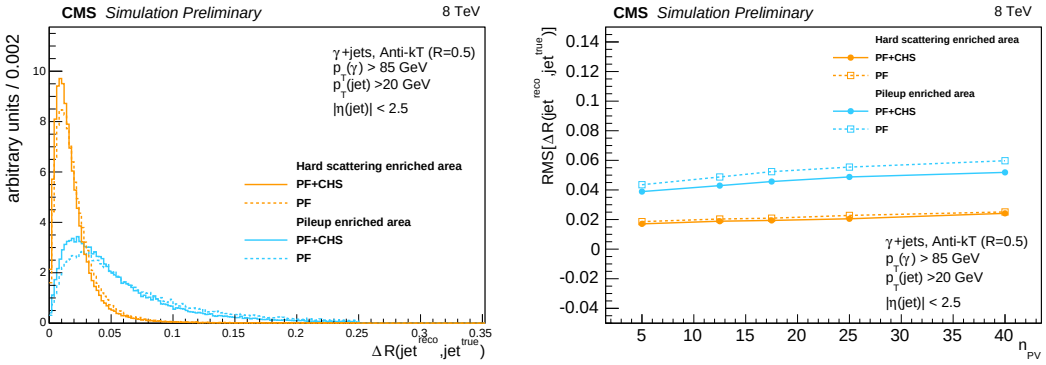

Figure 4: (Left) Residual shifts $\Delta R(\text{reco}, \text{gen})$ between reconstructed and generated jets. (Right) The RMS of the residual shift $\Delta R(\text{reco}, \text{gen})$ versus number of primary vertices, demonstrating the relative improvement from CHS with increasing PU.

of charged hadrons needs information on charged particles and only affects the inner part of jets reconstructed at the edge of the tracker acceptance, hence biassing their direction out. The maximal bias for PF+CHS seen in Fig. 5 (right) at low p_T is -0.02, or about the width of a single ECAL crystal. At higher p_T the bias becomes negligible. Despite the η bias, no degradation in the η resolution is observed for PF+CHS with respect to PF jets. The bias around $|\eta| \sim 3$, visible whether CHS has been applied or not, is a feature of the detector granularity in the PF clustering.

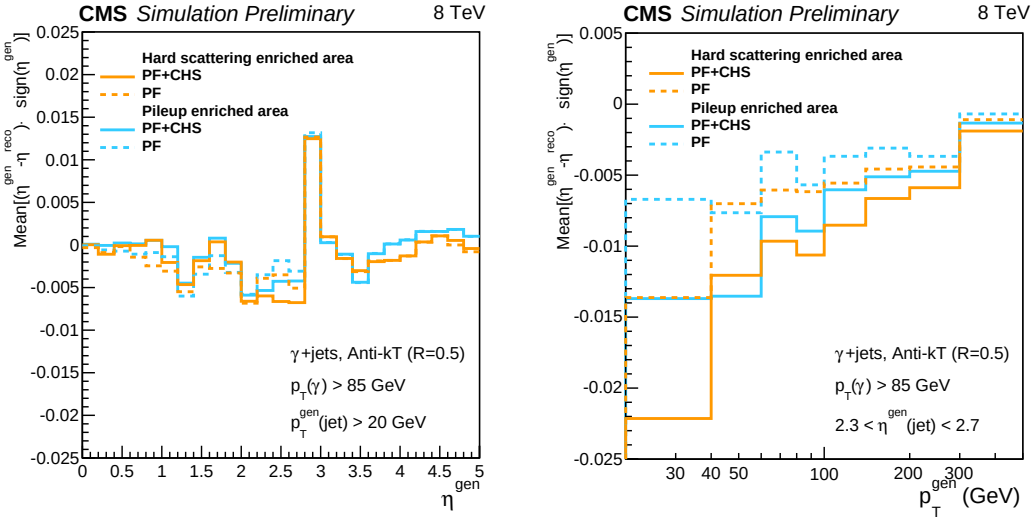

Figure 5: (Left) Mean of $(\eta^{\text{gen}} - \eta^{\text{reco}}) \cdot \text{sign}(\eta^{\text{gen}})$ with respect to η^{gen}, showing biases generated by discontinuous pileup energy density at the tracker edge at $|\eta| \approx 2.5$ and by changes in detector granularity at $|\eta| \approx 3.0$. (Right) Zoom into the tracker edge region showing bias versus $p_{\text{T}}^{\text{gen}}$ becoming neglible at high p_T.

To summarize, from these studies we find that CHS reduces the effect of pileup on reconstructed jets and improves both p_{T} and angular resolution. Additionally, CHS also reduces the rate of low p_{T} jets formed purely from pileup in the tracker region. The procedure does introduce a small η bias for jets at the tracker boundaries for low p_{T} jets.

4.3 Data-MC comparisons

In this section, the selected data events, corresponding to 19.7 fb^{-1} from the full Run I dataset, are compared to simulation. After the selection, described in 4.1, the main non-γ+jets background is due to QCD multijet events, which represent about half of the sample at low reconstructed photon p_{T} and about 30% at high reconstructed photon p_{T}. In the simulation, the γ+jets and QCD multijet events are generated and their relative contributions are determined according to their cross-sections [18].

Figure 6 shows the response in the hard scattering region computed with the "Missing-E_T Projection Fraction" method (MPF), *i.e.*:

$$R_{MPF} = 1 + \frac{\overrightarrow{MET} \cdot \vec{p}_T(\gamma)}{\vec{p}_T^{\,2}(\gamma)} \tag{1}$$

The application of CHS does not significantly affect the mean of the MPF response, but the resolution improves particularly at high pileup, as seen in Fig. 6 (right). A slightly worse resolution is observed in data with respect to simulation, however the relative trends between PF and PF+CHS are similar in data and simulation, and confirm the performance improvement from using CHS at high pileup.

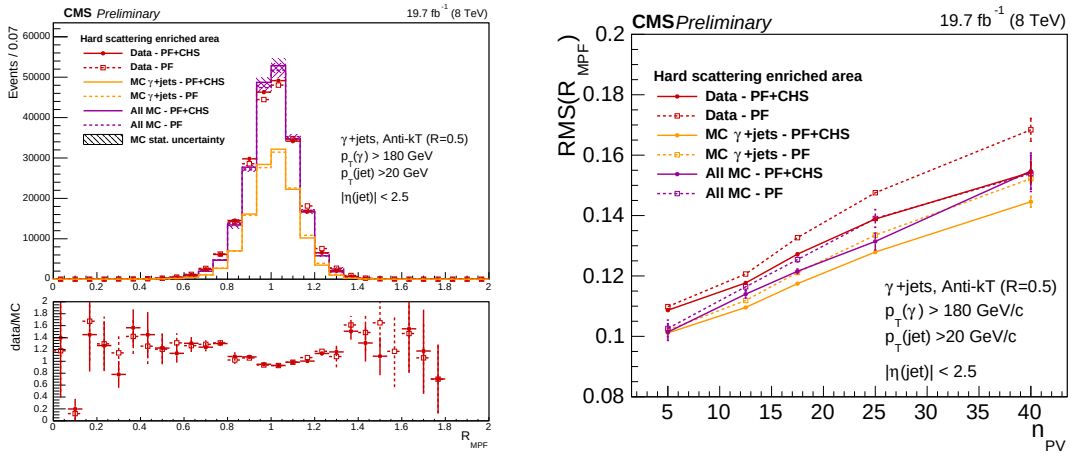

Figure 6: (Left) MPF response of jets with PF and PF+CHS in data and simulation. The hashed area corresponds to the MC statistical uncertainty. (Right) RMS of MPF response versus pileup for PF and PF+CHS compared between data and simulation. In simulation, "All MC" includes the contribution from γ+jets and QCD multijets events.

5 Grooming algorithms

Grooming, the systematic removal of a subset of the jet constituents, has been introduced in [26] and is intended to remove soft and wide-angle radiation from the jet. It is typically used to reduce the overall jet mass of QCD (quark- and gluon-initiated) jets while preserving the larger jet mass for jets originating from heavy particles such as the top quark and W/Z/H bosons or new physics. Additionally, grooming, in the presence of pileup, can be used to reduce the dependence of jet mass on pileup activity. It should be noted that jet grooming, in general, alters the soft structure of the jet while other jet structure observables may rely on this soft structure. For example, it was found in [2] that the jet shape N-subjettiness [27] computed from the groomed quantities is a less discriminant observable than the ungroomed jet observable. Thus we focus on the performance of jet groomers on the jet mass.

In this section, we explore the effect of grooming as a pileup mitigation method on large-R jets (R=0.8). We consider the grooming methods: pruning, trimming, modified mass drop tagger and soft drop.

The pruning algorithm reclusters the constituents of the jet through the Cambridge-Aachen (CA) algorithm [28], using the same distance parameter. At each step in the clustering algorithm, the softer of the two particles i and j to be merged is removed when the following conditions are met:

$$z_{ij} = \frac{\min(p_{\mathrm{T}i}, p_{\mathrm{T}j})}{p_{\mathrm{T}i} + p_{\mathrm{T}j}} < z_{\mathrm{cut}} \tag{2}$$

$$\Delta R_{ij} > D_{\mathrm{cut}} = \frac{2 \times r_{\mathrm{cut}} \times m_J}{p_{\mathrm{T}}} \tag{3}$$

where m_J and p_{T} are the mass and transverse momentum of the originally-clustered jet, and z_{cut} and r_{cut} are parameters of the algorithm.

Trimming ignores particles within a jet that fall below a dynamic threshold in p_{T}. It reclusters the constituents of the jet using the kT algorithm with a radius r_{sub}, accepting only the subjets that have $p_{\mathrm{Tsub}} > p_{\mathrm{Tfrac}}\,\lambda_{\mathrm{hard}}$, where $p_{\mathrm{T\ frac}}$ is a dimensionless cutoff parameter, and λ_{hard} is some hard QCD scale chosen to equal the p_{T} of the original jet.

Soft-drop and modified mass drop tagger (MMDT) decluster the jet recursively to remove soft and wide angle radiation from the jet. The jet is reclustered using the CA algorithm. Then the jet is declustered and at each step, subjets j_1 and j_2 are defined, and the following condition is defined:

$$\frac{\min(p_{\mathrm{T}j1}, p_{\mathrm{T}j2})}{p_{\mathrm{T}j1} + p_{\mathrm{T}j2}} > z_{\mathrm{cut}} \times \left(\frac{\Delta R_{12}}{R_0}\right)^{\beta} \tag{4}$$

where the algorithm parameters are z_{cut} and β and R_0 is the distance parameter R of the original jet finding algorithm. If the condition is met, the declustering continues, otherwise only the leading p_{T} subjet is kept. In the case when $\beta = 0$, soft drop can be considered a generalization of the modified mass drop tagger.

The (groomed) masses are corrected for pileup using a four-vector "safe" subtraction [29]. It is an extension of area subtraction including a correction for jet masses [30, 31]:

$$p^{\mu}_{sub} = p^{\mu} - \rho A^{\mu} - \rho_m A^{\mu}_m \tag{5}$$

where ρ and ρ_m are measures of the average pileup density and the ρ_m term is required due to the non-zero hadron masses of the particle flow inputs. In the case of PF+CHS inputs, care is required to estimate $\rho_{(m)}$ from neutrals only in the central region to correct jets with $|\eta| < 2.5$ and use the $\rho_{(m)}$ for the full η acceptance from PF inputs to correct forward PF+CHS jets. In the cases of soft drop, modified mass drop tagger, and trimming, the four-vector subtraction corrects the jet p_{T} and mass at each step in the algorithm. For pruning, the correction is applied to the final product using the pruned jet area.

The parameters for the grooming algorithms explored in this study are summarized in Table 1. For each grooming algorithm, a default set of parameters are chosen to be consistent with the previous CMS study [32] which defined parameters based on the original phenomenological studies. Those parameter choices are $z_{\mathrm{cut}} = 0.1$, $r_{\mathrm{cut}} = 0.5$ for pruning and $r_{\mathrm{sub}} = 0.2$, $p_{\mathrm{T\ frac}} = 0.03$ for trimming. We choose additional values of the pruning and trimming parameters which are more and less aggressive in removing the jet's soft constituents than the default parameters. For soft drop, parameters are chosen based on the suggestion of [9].

grooming algorithm	parameter(s)
Trimming [7]	$r_{\text{sub}} = 0.2$, $p_{\text{T frac}} = 0.05$ $r_{\text{sub}} = 0.2$, $p_{\text{T frac}} = 0.03$ $r_{\text{sub}} = 0.1$, $p_{\text{T frac}} = 0.03$ $r_{\text{sub}} = 0.3$, $p_{\text{T frac}} = 0.03$
Pruning [8]	$z_{\text{cut}} = 0.1$, $r_{\text{cut}} = 0.5$ $z_{\text{cut}} = 0.05$, $r_{\text{cut}} = 0.5$ $z_{\text{cut}} = 0.1$, $r_{\text{cut}} = 0.75$ $z_{\text{cut}} = 0.05$, $r_{\text{cut}} = 0.75$
Soft drop [9]/MMDT [10]	$z_{\text{cut}} = 0.1$,$\beta = 0$ $z_{\text{cut}} = 0.1$,$\beta = 1$ $z_{\text{cut}} = 0.1$,$\beta = 2$

Table 1: Summary of grooming parameters considered.

5.1 Physics objects and event selection

For this study, we consider the dijet event topology. The grooming algorithms are studied for large-R jets clustered with the anti-kT algorithm with R = 0.8. We consider the jets which are reconstructed from particle flow inputs with and without CHS applied. We consider the leading jet in background multijet events and signal WW events where the corrected p_{T} of the jet is $p_{\text{T}} > 300\,\text{GeV}$.

5.2 Higher pileup studies for LHC Run II

As preparation for LHC Run II, we study the various groomers with higher pileup scenarios expected in LHC Run II. The studies are performed with simulation only. We consider primarily the jet mass distributions after grooming is applied for both background QCD jets and signal W jets. In both cases, we consider the several metrics for judging the merits of each grooming algorithm and choice of parameters.

- The first metric is the pileup sensitivity of the algorithm and the preference is for algorithms more robust against the effects of pileup.
- We also consider the accuracy of the reconstruction with each algorithm, typically by evaluating the mass *response* which compares the reconstructed jet mass with respect to the particle level generator jet mass, $m_{\text{reco}} - m_{\text{gen}}$. In this case, the reconstructed jet is matched ($\Delta R < 0.3$) to a particle level jet. The core mass response resolution is measured with a fit to a Gaussian function while the RMS of the distribution is also computed to evaluate the effect of the tails of the distributions.
- The final metric is the performance in separating background from signal. In the most general terms, this translates into narrower resonance resolution for the signal, in our case it is the W mass peak resolution, and reducing the amount of background in the typical signal region.

There need not be one grooming algorithm which outperforms the others in every metric. The goal is to understand the performance of each grooming algorithm. For applications of the different groomers, for example in searches for new physics, the type of search will dictate which groomer should be used.

First, in Fig. 7, we show the mass distributions themselves for each of the groomers, integrated over all n_{PV} in order to understand the general behavior of each of the groomers. The groomers

we consider more "aggressive" such as soft drop ($\beta = 0$), pruning ($z_{cut} = 0.1$, $r_{cut} = 0.5$) and trimming ($r_{\text{sub}} = 0.1$, $p_{\text{T frac}} = 0.03$) tend to push the bulk of the QCD jets down to smaller jet masses although they typically have larger tails in the high mass regime. On the contrary, less aggressive groomers such as trimming ($r_{\text{sub}} = 0.2$, $p_{\text{T frac}} = 0.03$) and soft drop ($\beta = 2$) have a smaller tail though the bulk of the distribution is typically a bit larger in jet mass. The choice of the groomer to use would be dependent on the type of search being performed.

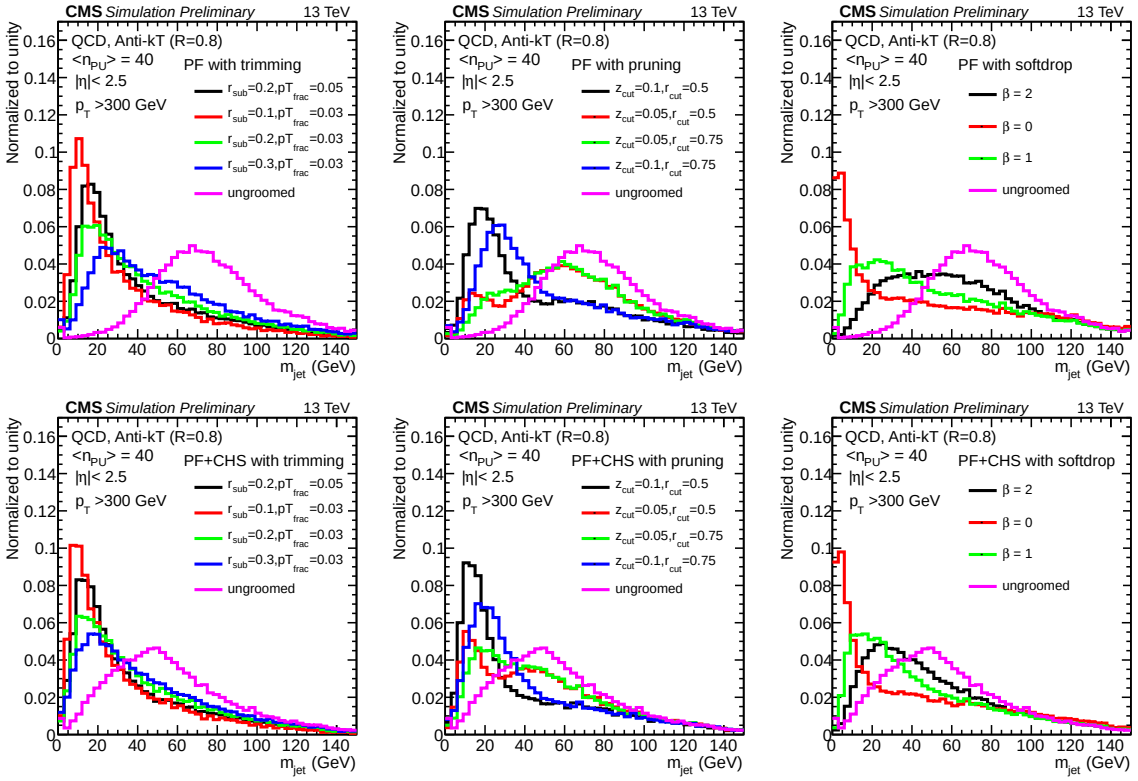

Figure 7: Jet mass distributions for the various groomers considered.

Now, we evaluate the pileup dependence performance of groomers based on particle flow input collection with and without CHS to understand the effect. We show the average jet mass for PF and CHS background QCD jets in Fig. 8. The left column shows the average jet mass as a function of n_{PV} for jets using particle flow inputs. The right column shows the average jet mass as a function of the n_{PV} for jets using particle flow inputs including CHS. We see generally that the CHS jet masses are more stable against pileup. For the trimming and soft drop groomers, the average jet mass is relatively unchanged between PF and PF+CHS which is due to the way that the four-vector safe subtractor is applied to those algorithms as compared to the pruning algorithm. Generally the pruning algorithm shows the most sensitivity to pileup with the trimming and soft drop groomers are more stable in average jet mass.

Given the similar or improved performance of the PF+CHS algorithm with respect to PF, we compare the performance of the various groomers for several different parameters using the PF+CHS inputs. In Fig. 9, we present the RMS of the jet mass response as a function of n_{PV} for background (left) and signal (right) jets for various groomers as a function of the number of primary vertices. In the case of the signal, we show both the σ of the Gaussian fit and the RMS of the distribution in order to characterize the core and the tails of the distributions. The RMS and σ of the $(m_{\text{reco}} - m_{\text{gen}})$ distribution are evaluated in the range [-100,100] GeV. We can see that the trimming algorithm is slightly improved in jet mass resolution with respect to the other algorithms. Additionally, we find that it has the least amount of tails as the RMS of the

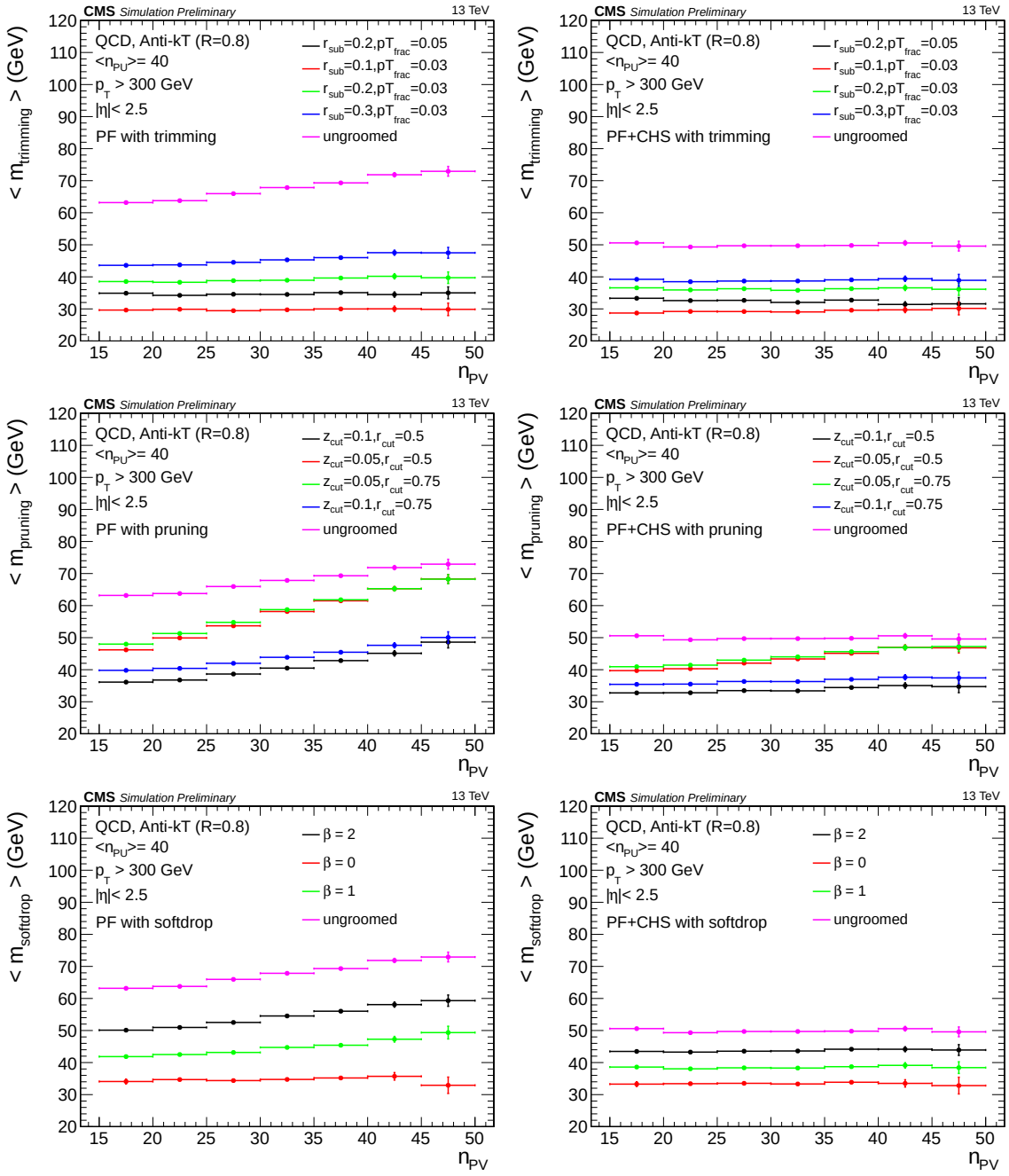

Figure 8: Pileup dependence versus n_{PV} of the average jet mass for PF jets (left) and PF+CHS jets (right) for several grooming algorithms and parameters. The top row is trimmed jets, middle row is pruned jets and bottom row is jets with soft drop applied.

jet mass distributions are smaller.

To better understand the effect of the jet mass response, we show the distributions integrated over all n_{PV}. This is shown in Fig. 10. It is clearer now here that there are longer tails in the jet mass response for the pruning algorithm. The trimming algorithm has less of an issue, although we should note that the trimming algorithm also has the largest offset in the mean of the mass response distribution.

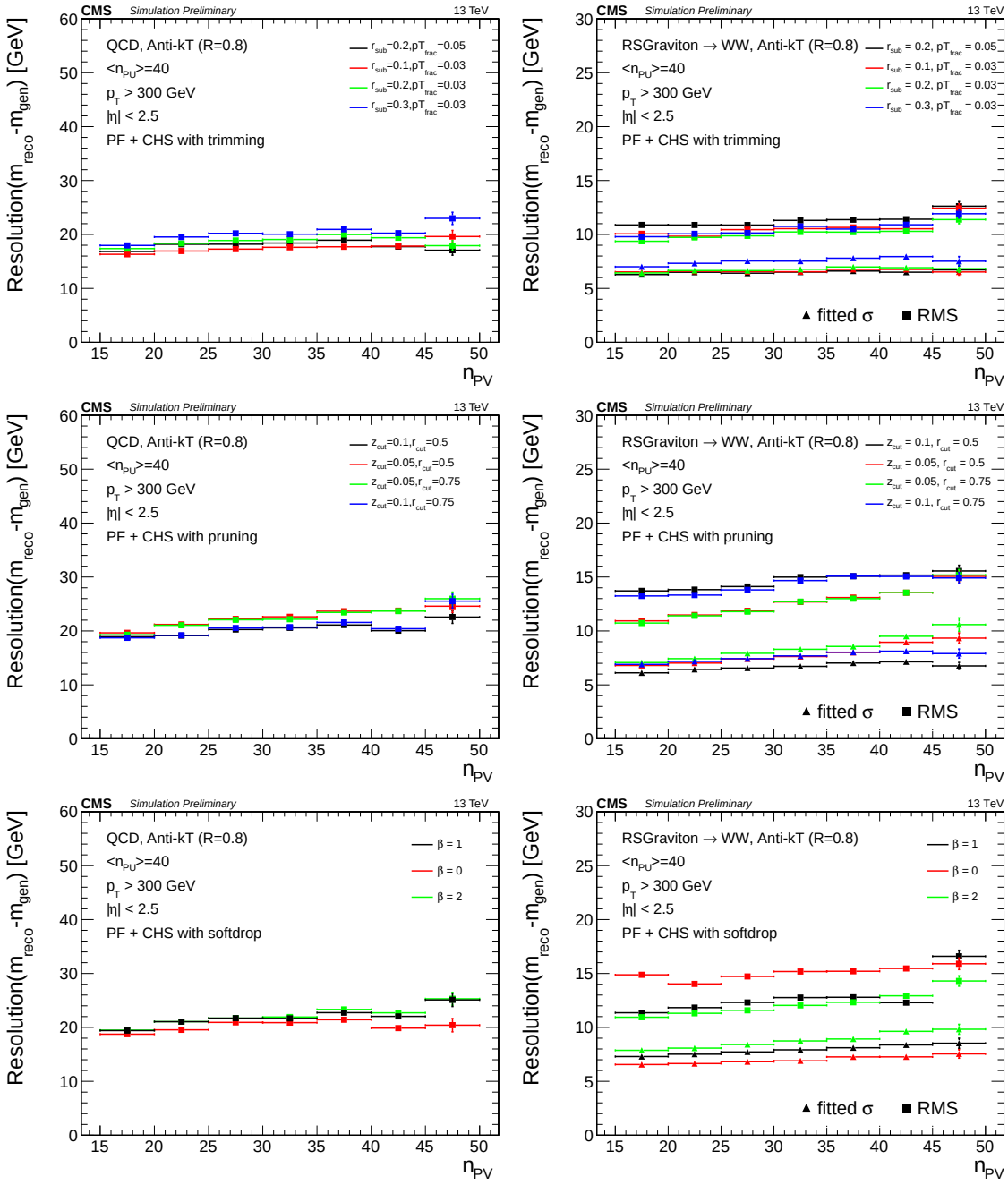

Figure 9: Pileup dependence versus n_{PV} of the mass resolution for QCD jets (left) and jets matched to generated W bosons (right) for various parameters of the grooming algorithms. For jets matched to W bosons, both the RMS and the σ from a Gaussian fit to the $(m_{\text{reco}} - m_{\text{gen}})$ distribution are reported.

A summary of the W mass resolution for signal W jets reconstructed using different grooming parameters is reported in Fig. 11. For comparison, the ungroomed mass m is shown with and without four-vector safe subtraction. The resolution is characterized both in terms of σ from a Gaussian fit of the W mass peak and in terms of RMS, in order to give an indications of the tails of the mass distribution. The σ is obtained by fitting the mass distribution in a window $\pm\Delta m$ centered on the average mass, where Δm is equal to the RMS on the full mass range distribution; the RMS estimator for the resolution is taken as a truncated RMS in a mass range

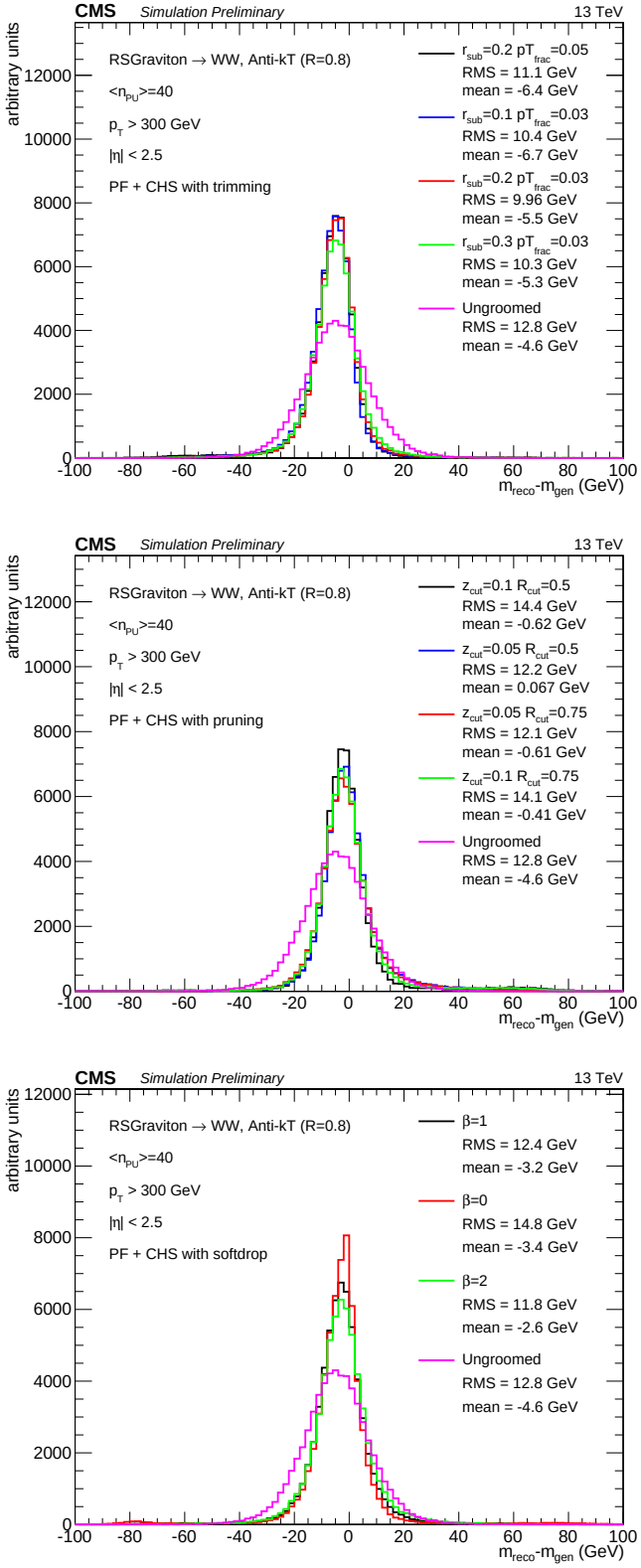

Figure 10: Jet mass response for signal W jets for various grooming algorithms: trimming (top), pruning (middle), soft drop (bottom).

of $\pm 3\sigma$ around the fitted mean. The W mass resolution is improved in all cases for PF+CHS as

compared to the PF inputs.

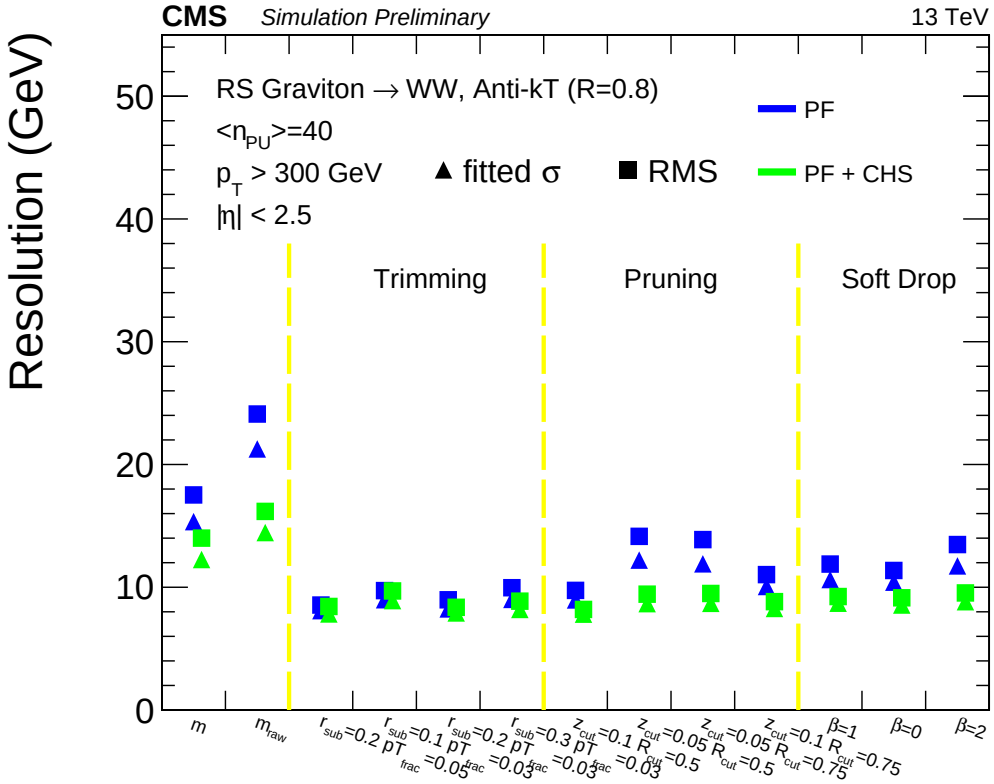

Figure 11: Comparison of PF and CHS W mass resolution for signal W jets reconstructed using different grooming parameters. m is the ungroomed jet mass with four-vector safe subtraction and m_{raw} is the ungroomed and uncorrected jet mass.

5.3 Data-MC comparisons from LHC Run I

With the current available LHC Run I data sample, we can compare the simulated distribution of groomed masses to the data. We apply a basic dijet selection with at least one jet with $p_{\mathrm{T}} > 400\,\mathrm{GeV}$, the dijet mass m_{jj} >900 GeV and finally we require $|\Delta\eta_{jj}| < 1.2$. The dijet mass requirement ensures >99% efficiency of the trigger.

Using the data from the end of 2012, corresponding to an integrated luminosity of 8 fb^{-1}, we make a comparison of the leading jet groomed mass in data and simulation for PF+CHS jets. In Fig. 12, we show the data to MC comparison of the jet mass for the trimming, pruning and soft drop algorithms. Generally the agreement is reasonable where the largest disagreement comes in the low jet mass region where non-perturbative effects are the largest.

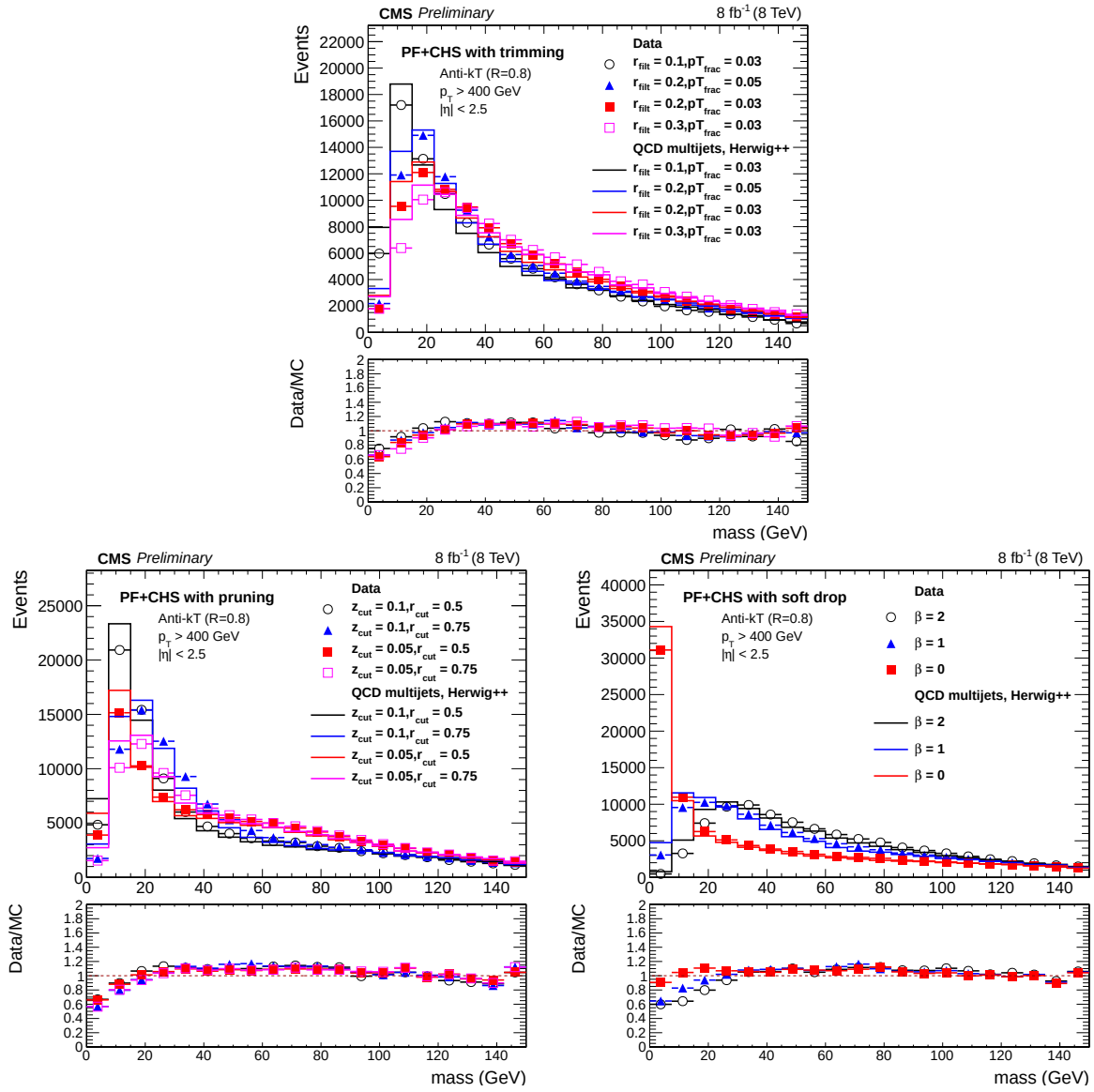

Figure 12: Jet mass distributions for QCD jets with $p_{\mathrm{T}} > 400$ GeV in data and simulation for various grooming algorithms: trimming (top), pruning (bottom left), soft drop (bottom right)

6 Pileup mitigation tools

In Sections 4 and 5, we studied the effect of tracking and local shape information, respectively, as a tool for mitigating the effects of pileup on jets. In this section we explore various new techniques which are aimed at further reducing the pileup dependence of jets and improving over the techniques described in the previous sections. We consider three algorithms: constituent subtraction, jet cleansing, and pileup per particle identification (PUPPI).

Constituent subtraction is a natural extension of the generic subtraction techniques to the smallest distance scales within a jet. Rather than subtracting a $\rho \times A$ quantity from a jet, the area is distributed with ghost particles whose total momenta defines the total amount of p_{T} to be subtracted. By defining a matching scheme to specify which ghosts are closest to which particles, one can subtract a unique amount of pileup from each particle. In performing subtraction at the particle level, it becomes natural to correct generic jet shapes in addition to jet p_{T} and jet mass.

Jet cleansing uses both local shape information and tracking information to correct a jet at the subjet level. It relies on using the local distribution of charged particles for the leading vertex and pileup. A number of subjets are defined, as in trimming, and the p_{T} of each subject is characterized as:

$$p_T^{\mathrm{tot}} = \frac{p_T^{C,PU}}{\gamma_0} + \frac{p_T^{C,LV}}{\gamma_1} \tag{6}$$

where PU and LV are the contributions from pileup and leading vertex, respectively; and $\gamma_0 \equiv p_T^{C,PU}/p_T^{PU}$ and $\gamma_1 \equiv p_T^{C,LV}/p_T^{LV}$ are the charged-to-total p_{T} fractions and are generally unknown. There are multiple schemes proposed by the authors to estimate γ_0 and γ_1. We study the various performances in some detail and find a suitable working point for linear jet cleansing (defined in [12]) which assumes a global value of $\gamma_0 \equiv \bar{\gamma_0}$. For linear jet cleansing we choose the parameters where the subjet R = 0.2 and $\bar{\gamma_0} = 0.55$.

PUPPI attempts to use local shape information, event pileup properties and tracking information together to reduce the effect of pileup on jet observables. Unlike the two other methods, PUPPI operates on the inputs to the jet clustering algorithm, thus before the jets themselves are formed. A local variable α is computed which contrasts the collinear structure of QCD with the soft diffuse radiation coming from pileup. The local shape for charged pileup, assumed as a proxy for all pileup particles, is used on an event-by-event basis to calculate a weight for each particle. The weights describe the degree to which particles are pileup-like and are used to rescale their four-momenta, superseding the need for jet-based corrections.

As discussed in [13], various definitions of the discriminating variable α are possible. In this study, we adopted a configuration with a different definition of α for particles in the central ($|\eta| < 2.5$) and forward region ($|\eta| > 2.5$) of the detector, where tracking information is not available. The choice is optimized in order to obtain the best discriminating power between pileup and particles from the hard scattering vertex in the pileup scenario under study.
In the central region, the shape variable for a given particle i is defined as

$$\alpha_i = \log \sum_{\substack{j \in Ch,PV \\ j \neq i}} \left(\frac{p_{T,j}}{\Delta R_{ij}} \right)^2 \Theta(R_0 - \Delta R_{ij}) \tag{7}$$

where Θ is the step function, i refers to the particle in question and j to the neighboring charged particles from the primary vertex within a cone of radius R_0. We consider charged particles as coming from the primary vertex those whose track is associated to the leading vertex of the

event or is unassociated but with d_z <0.3 cm, where d_z is the distance along the z axis with respect to the leading vertex. In the forward region, two variables are used:

$$\alpha_i = \log \sum_{j \neq i} \frac{p_{T,j}}{\Delta R_{ij}} \Theta(R_0 - \Delta R_{ij}) \tag{8}$$

and

$$\alpha_i = \log \sum_{j \neq i} p_{T,j} \Theta(R_0 - \Delta R_{ij}). \tag{9}$$

where i refers to the particle in question and j to all neighbouring particles within R_0. We found that in the forward region, characterized by a lower detector granularity, the usage of both the variables defined in Eq. 8 and Eq. 9 improves the performance. A χ^2 approximation

$$\chi^2_i = \frac{(\alpha_i - \bar{\alpha}_{PU})^2}{RMS^2_{PU}} \tag{10}$$

where $\bar{\alpha}_{PU}$ is the median value of the α_i distribution for pileup particles in the event and RMS_{PU} is the corresponding RMS, is used to determine the probability of a particle to be from pileup. In the tracker region, $\bar{\alpha}_{PU}$ and RMS_{PU} are calculated using all charged pileup particles (i.e. all charged particles not from PV), while in the forward region they are calculated using all the particles in the event. The pseudorapidity dependence of α_{PU} and RMS_{PU} is accounted for by computing their values separately in three pseudorapidity bins ($0 < |\eta| < 2.5$, $2.5 < |\eta| < 3$ and $|\eta| > 3$). In the forward region, where the two variables defined in Eq. 8 and Eq. 9 are used, the corresponding χ^2 are summed.
The algorithm parameters choices are similar to what is recommended in [13]. The radius of the cone R_0 is set to 0.3. Particle weights w_i are required to be larger than 0.01 and a cut on the minimum scaled p_{T} of the neutral particles is applied: $w_i \cdot p_{\mathrm{T}i} > (0.2 + 0.02 \cdot n_{PV})$ GeV, where n_{PV} is the reconstructed vertex multiplicity in the event. This cut is tuned as a function of n_{PV} in order to make the jet p_{T} and mass response close to unity and to improve the p_{T} and mass response stability against pileup.

6.1 Physics objects and event selection

The performances of the different algorithms are compared for jets clustered starting from particle flow candidates and using the anti-kT algorithm with R=0.8. For PF and PF+CHS jets, the jet four momenta are corrected with the safe 4-vector area subtraction. The leading large-R jet in QCD multijet events and in W jets from the graviton sample are considered with the corrected p_{T} in the range 200-600 GeV.

6.2 Higher pileup studies for LHC Run II

We explore the performance of these algorithms in the p_{T} observable as well as further jet substructure observables such as the jet mass, the groomed jet mass, and the N-subjettiness variable τ_2/τ_1.

The leading jet p_{T} distribution and response are compared in Fig. 13 for PF, CHS and PUPPI algorithms. The three algorithms show a comparable resolution for high p_{T} jets. Not much improvement in resolution is expected by PUPPI at high p_{T} as the effects of pileup are smaller.

In Fig. 14, the leading jet mass distribution and response for jets within $|\eta| < 2.5$ are shown for various algorithms. PUPPI provides the best mass resolution and response. Cleansed jets have also a good response, but slightly larger tails in the resolution as can be observed by comparing

the RMS and σ from a Gaussian fit of the m_{reco}-m_{gen} reported in Fig. 15. Constituent subtraction brings an improvement over PF+CHS safe subtraction, but does not perform as well as PUPPI or cleansing. A summary of the mass resolution obtained using the different pileup mitigation approaches is reported in Fig. 15.

The dependence on pileup of the reconstructed mass and resolution is shown in Fig. 16 for W jets. In Fig. 16-left we can see that PF+CHS provides a stable response against pileup, but it suffers from the largest bias in the reconstructed mass. Constituent subtraction improves both the average response and the resolution over PF+CHS with safe area subtraction, even if with a small dependence of the mass response on pileup. Cleansing presents a trend in the mass response as a function of n_{PV} similar to PUPPI and PF+CHS with constituent subtraction, with slightly worse resolution. PUPPI provides the best mass resolution and shows a resonable stability against pileup. The residual slight pileup dependence of PUPPI could be reduced by further tuning the algorithm parameters.

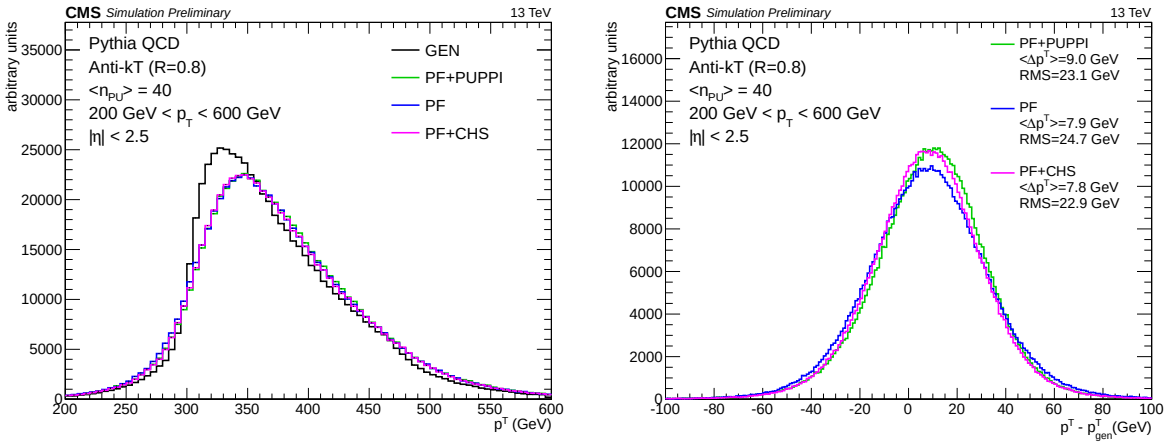

Figure 13: Jet p_{T} distribution (left) and resolution (right) for the leading jet in QCD events.

Figure 17 presents the distribution of τ_2/τ_1 for QCD jets and W jets, demonstrating that both PUPPI and constituent subtraction are also effective in correcting jet shapes bringing them closer to their particle level value. The τ_2/τ_1 distribution is shown also for events with the pruned mass (z_{cut} =0.1,R_{cut} =0.5) between 60 and 100 GeV. This cut removes the contribution from unmerged W jets. The improved τ_2/τ_1 reconstruction does not necessarily improve the discrimination between signal W jets and QCD jets, however, as illustrated in Fig. 18, the dependence on pileup of this variable is mitigated by PUPPI and constituent subtraction as compared to PF and PF+CHS constituents, making it easier to apply cuts to substructure observables and get stable performance versus pileup.

It is also possible to combine the jet-grooming techniques described in Sec. 5 with the pileup removal techniques described in this chapter to further improve the performance.

A summary of the jet mass resolution for PUPPI in comparison with PF and PF+CHS jets, combined with grooming techniques, is shown in Fig. 19 for different choices of the grooming parameters. Both the RMS and σ from a Gaussian fit of the response distribution m_{reco}-m_{gen} are reported in order to have an estimate of the effect of the tails in the distributions. First of all, we observe that PUPPI shows overall the best mass resolution. This is the case even for the ungroomed mass, as visible from the first two bins of Fig. 19 where the ungroomed mass with and without four vector safe area subtraction are shown. The ungroomed mass resolutions with and without four vector safe area subtraction for PUPPI jets are furthermore very similar, which is consistent with the fact that PUPPI is by construction removing most of the

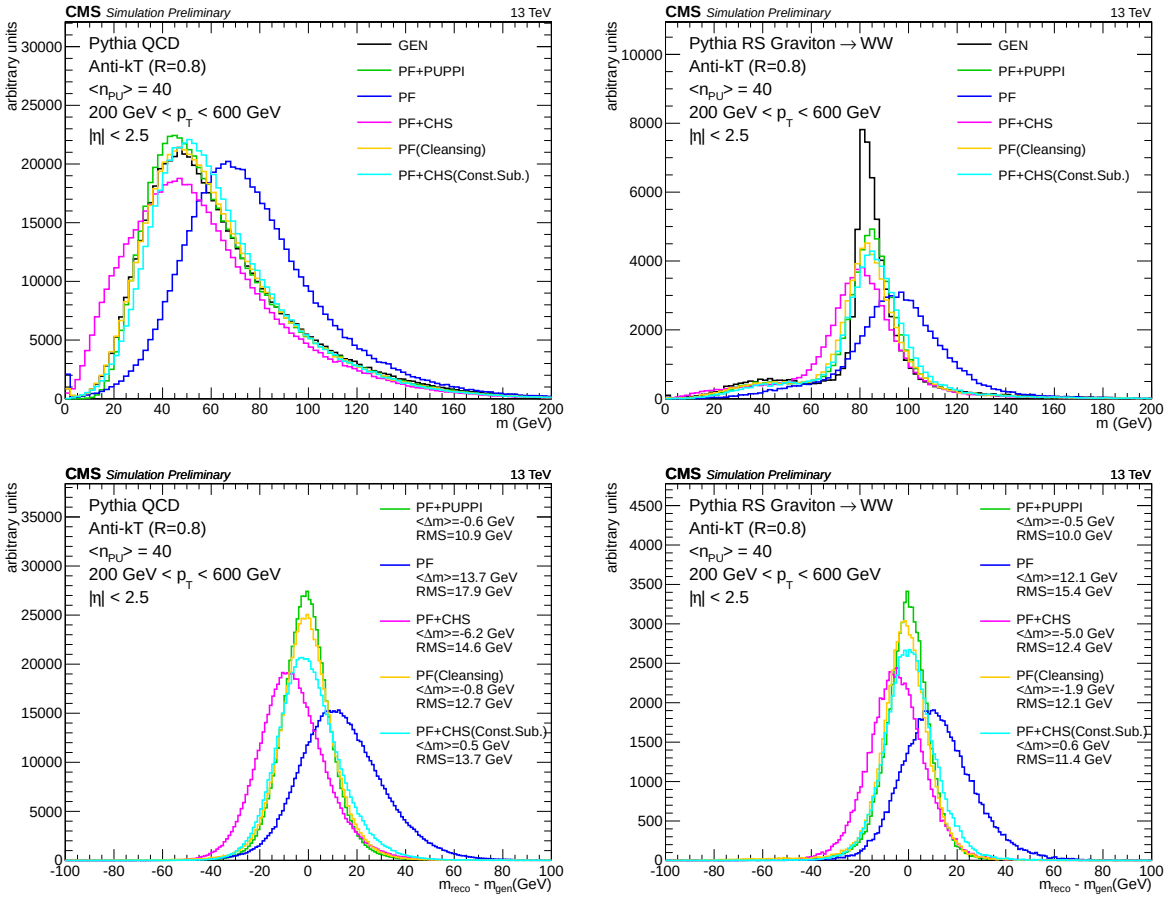

Figure 14: Comparison of the leading jet mass distribution (top) and response (bottom) for different algorithms in QCD multijet events (left) and for W jets from the decay of a RS graviton (right).

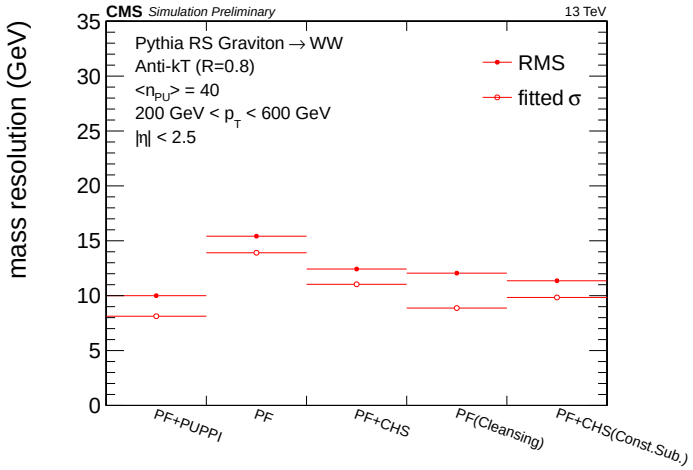

Figure 15: W jet mass resolution comparison for different pileup mitigation algorithms; both the RMS and σ from a gaussian fit to the distribution of the difference between reconstructed and particle level mass are quoted.

pileup contribution from the inputs to the jet clustering. While grooming brings a substantial improvement in the core jet mass resolution when applied to PF and PF+CHS jets, a smaller

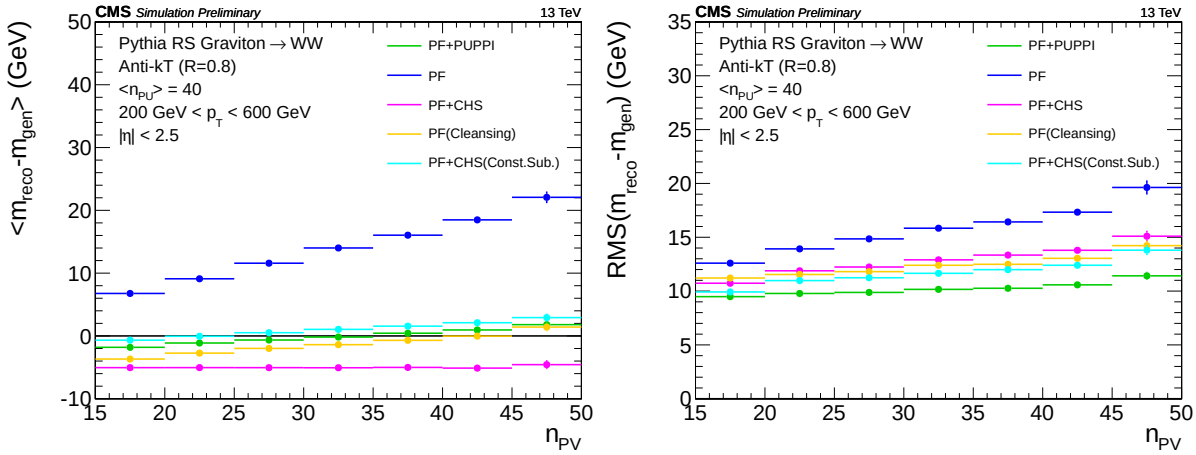

Figure 16: Mass response $< m_{\text{reco}} - m_{\text{gen}} >$ (left) and mass resolution quoted as RMS($m_{\text{reco}} - m_{\text{gen}}$) (right) for W jets as a function of the number reconstructed vertices.

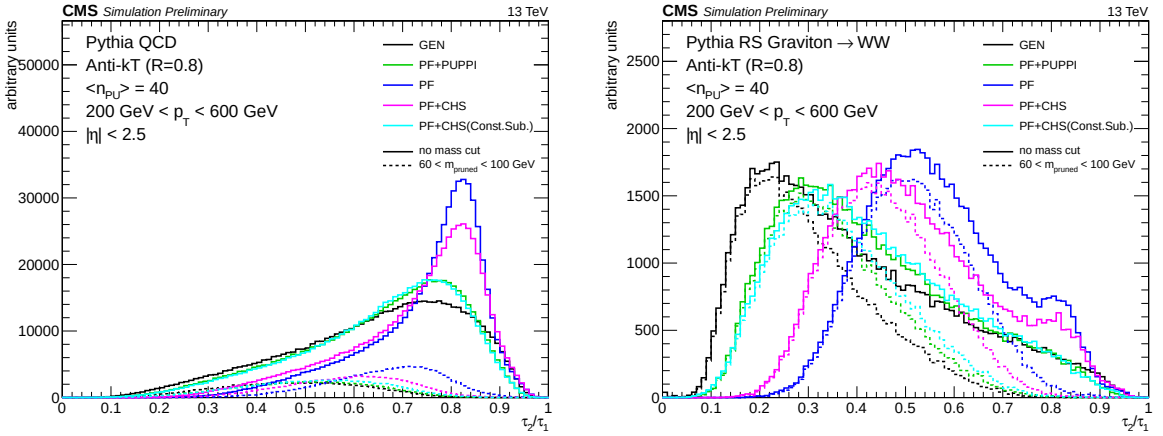

Figure 17: Leading jet N-subjettiness τ_2/τ_1 distribution: QCD jets (left) and W jets (right). The distribution is shown also after requiring the pruned mass to be in the range 60-100 GeV (dashed lines).

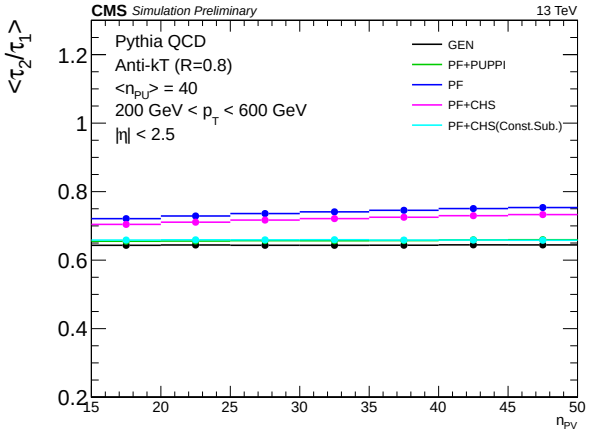

Figure 18: Average τ_2/τ_1 as a function of the number of reconstructed vertices.

improvement is observed for PUPPI jets. In particular, we observe that combining trimming with PUPPI does not improve the resolution with respect to the other groomers as much it

does when applied to PF or PF+CHS jets. We believe that this is due to the fact that trimming works with subjets instead that at the particle level, washing out some of the improvements one could expect. Finally, by comparing the resolution estimated from the RMS and σ values, it can be noticed that, in some cases, grooming introduces larger tails in the response distribution. Trimming presents the smaller tails with respect to other groomers for all the parameters tested and for all the jet inputs (PF, PF+CHS or PUPPI). Moreover, we notice that for PUPPI jets the groomed mass tails are larger than the ungroomed mass ones, especially with pruning and soft drop.

To summarize, in this Section we have investigated the performance of a number of pileup mitigation algorithms (PUPPI, constituent subtraction, cleansing) in terms of p_{T}, mass and shape reconstruction comparing them with the standard techniques of PF and PF+CHS reconstruction with safe four vector area subtraction. All the methods considered show an improved jet mass resolution with respect to PF or PF+CHS, with PUPPI showing the best mass resolution along with an improved stability against pileup.

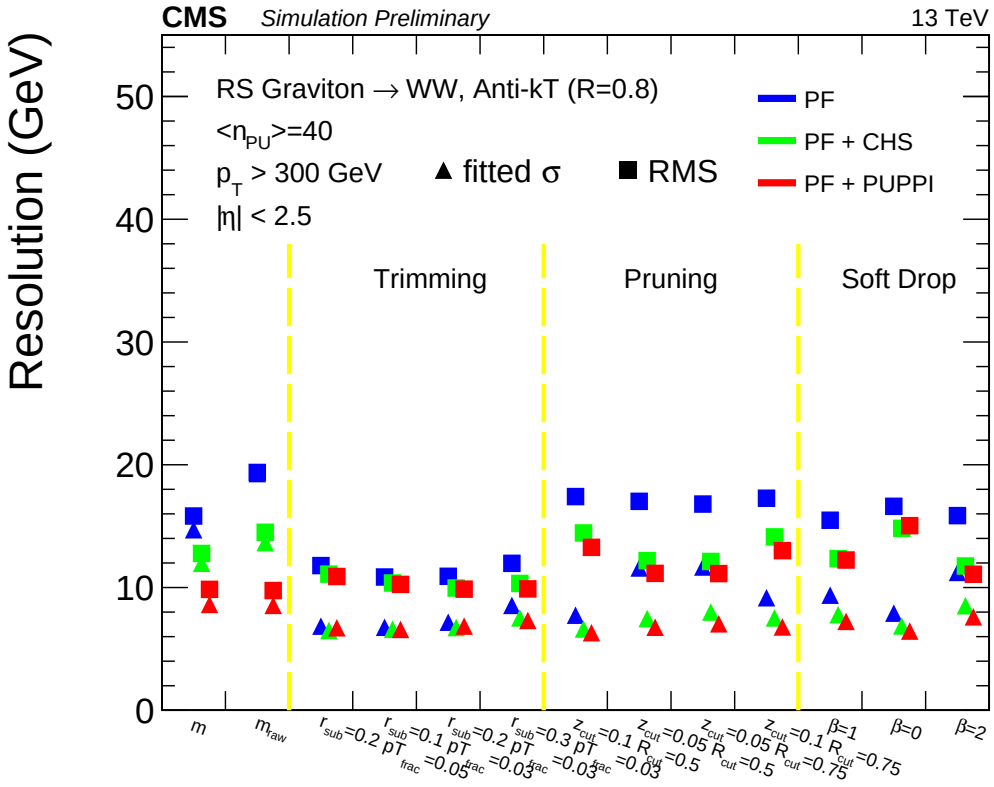

Figure 19: Comparison of PF, PF+CHS and PUPPI jet mass resolution for W jets reconstructed using different grooming parameters. The resolution is evaluated from the RMS (squares) and σ (triangles) of the m_{reco}-m_{gen} distribution, where for grooming results m_{gen} is the groomed mass at the particle level. The first two bins report the resolution of the ungroomed mass and of the raw mass (i.e. without safe four vector subtraction).

6.3 Data-MC comparisons from LHC Run I

We performed a comparison of some basic observables in data and MC simulation for jets reconstructed with the PUPPI algorithm. The data sample consists of high p_T jet events selected with the same requirements described in Sec. 5.3. In Fig. 20 the η and p_T distributions of the leading jet in the selected events are shown. In Fig. 21 the p_T distribution for the jets with p_T >40 GeV which are not the leading or sub-leading jet of the event is reported, separately for the central ($|\eta| < 2.5$) and forward ($|\eta| > 2.5$) regions of the detector, allowing to observe that the rate of PUPPI jets is lower than PF and PF+CHS due to lower pileup contamination. The dashed histogram denotes the subset of jets which do not have a matching jet at particle level in the simulation and thus are categorized as pileup jets. The leading jet mass and τ_2/τ_1 distributions are reported in Fig. 22 and the dependence of the average mass and τ_2/τ_1 on the number of reconstructed vertices in Fig. 23. A reasonably good agreement is observed for all the distributions.

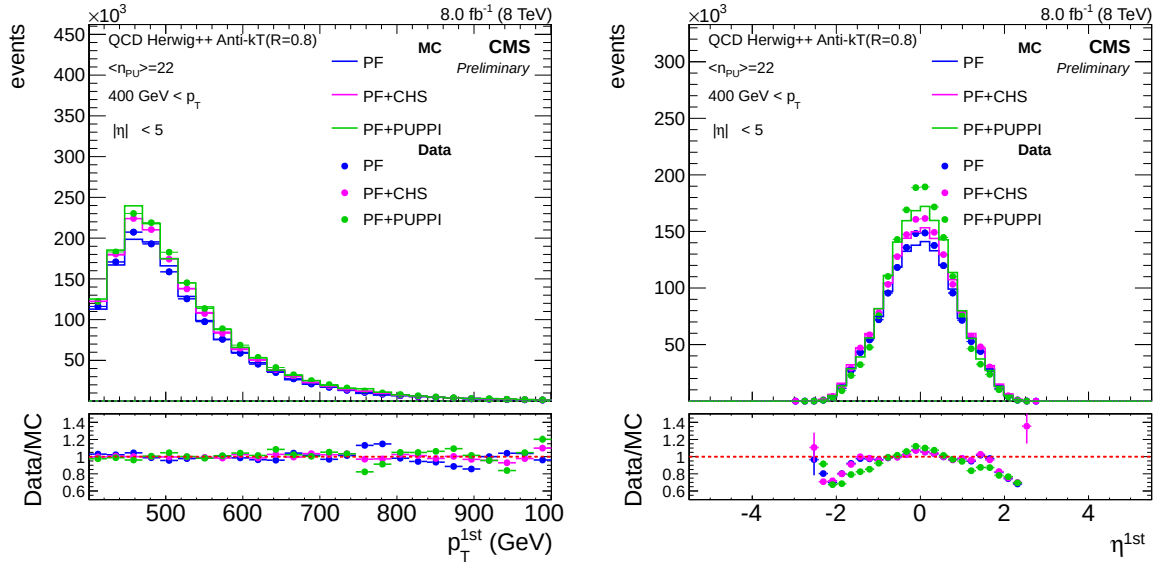

Figure 20: Leading jet transverse momentum (left) and pseudorapidity (right) distributions in high p_T multijet events for PF, PF+CHS and PUPPI jets. The dashed histogram denotes the subset of jets which do not have a matching jet at particle level in the simulation and thus are categorized as pileup jets.

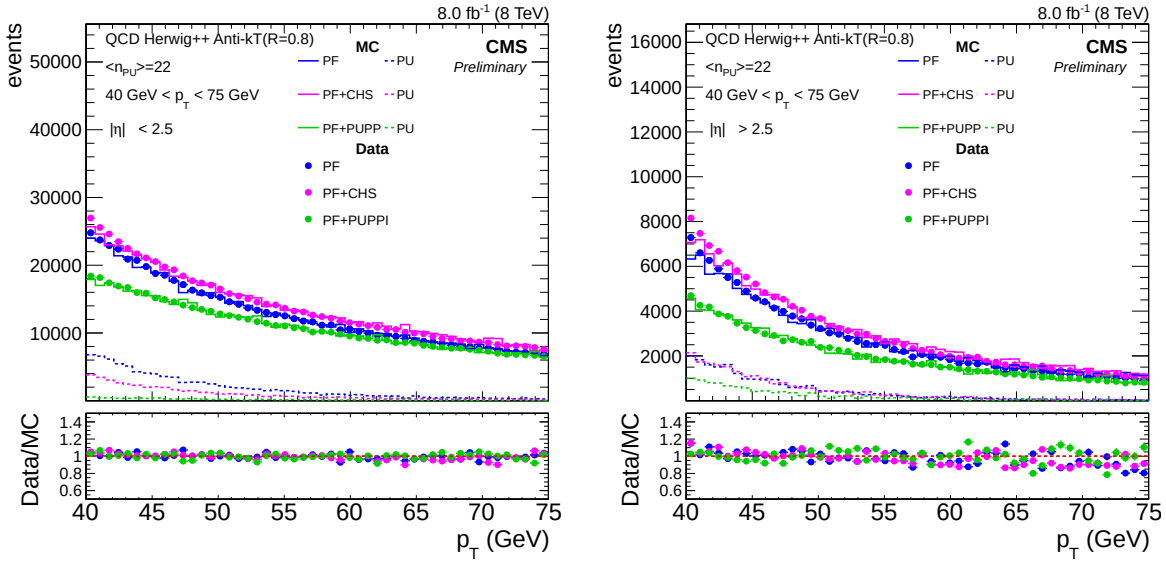

Figure 21: Transverse momentum distribution for jets in the central (left) and forward (right) pseudorapidity regions in multijet events for PF, PF+CHS and PUPPI jets. Only jets which are not the leading or subleading jet in the event are considered. The dashed histogram denotes the subset of jets which do not have a matching jet at particle level in the simulation and thus are categorized as pileup jets.

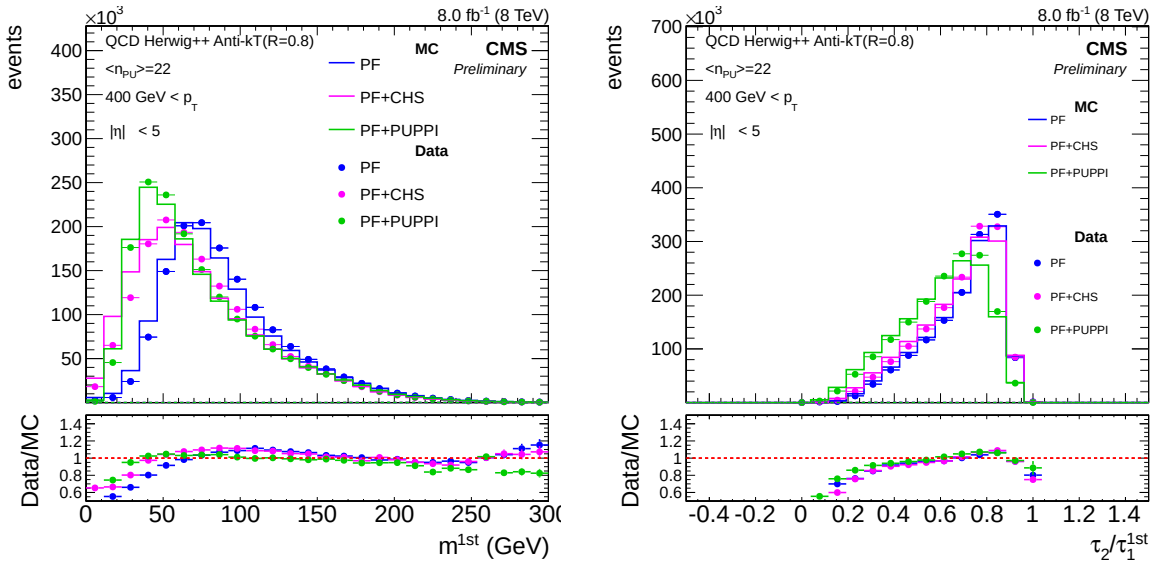

Figure 22: Leading jet mass distribution (left) and τ_2/τ_1 (right) in multijet events for PF, PF+CHS and PUPPI jets.

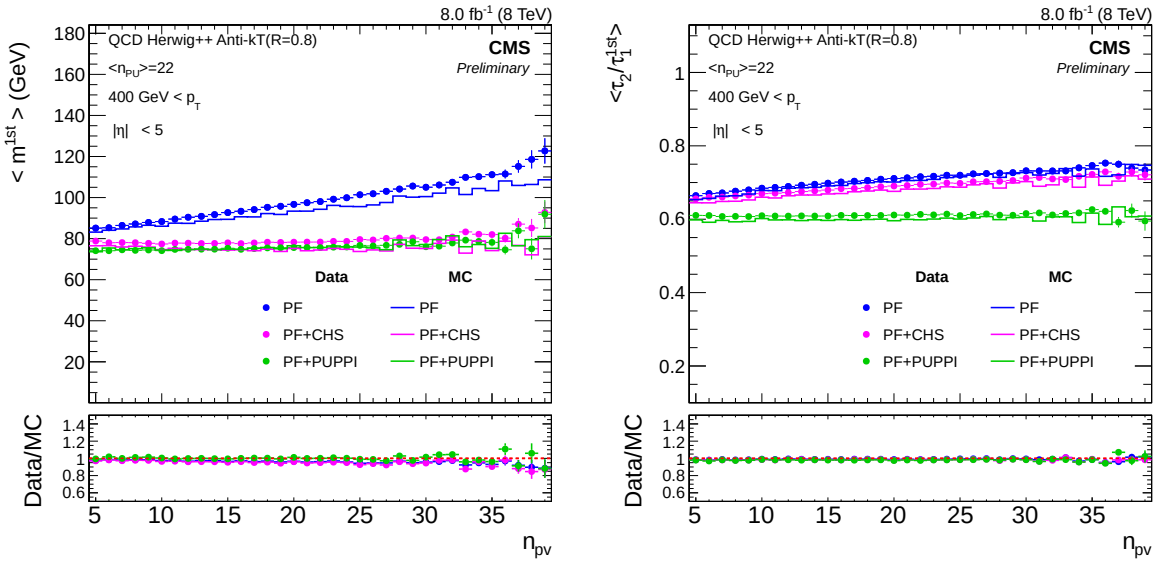

Figure 23: Leading jet average mass (left)and average τ_2/τ_1 (right) as a function of the number of reconstructed vertices in multijet events for PF, PF+CHS and PUPPI jets.

7 Conclusions

In this note, we explored a variety of methods of pileup mitigation for jets at CMS beyond the standard offset correction.

First, we studied the charged hadron subtraction (CHS) method which is targeted to remove charged particles from pileup from the particle flow inputs before jet clustering. We find that the rate of low p_T jets that are stochastically formed from pileup is reduced with CHS. An improvement in the jet p_T resolution and angular resolution was also observed, though a small η bias is introduced near the tracker boundary. The agreement between data and MC for jet reconstructed using the CHS approach is generally reasonable for jets coming from the hard scatter.

We investigated the performance of a number of jet grooming algorithms (pruning, trimming and soft drop), considering for each of them a few points in the parameter space. The effect of grooming was studied on large-R jets for jet substructure observables, in particular the groomed mass. Generally, we found that, along with CHS, the pileup dependence of jet mass is greatly reduced by grooming techniques. A comparison of the various algorithms and parameters shows that trimming has a slight improvement in the groomed jet mass resolution and is very stable against pileup for the pileup levels anticipated in early LHC Run II.

Finally, we studied some advanced methods for pileup mitigation: constituent subtraction, jet cleansing and pileup per particle identification (PUPPI). We investigated their performances on substructure observables in large-R jets and we found that all three methods improve over average subtraction techniques, even when including CHS. We found that generally PUPPI shows the best performances in terms of jet mass response and stability with respect to pileup.

The analysis of all these techniques demonstrates improvements over previous methods in higher pileup scenarios. All of the methods show promise for use in future LHC runs.

References

[1] CMS Collaboration Collaboration, "Performance of quark/gluon discrimination in 8 TeV pp data", Technical Report CMS-PAS-JME-13-002, CERN, Geneva, 2013.

[2] CMS Collaboration Collaboration, "Identifying Hadronically Decaying Vector Bosons Merged into a Single Jet", Technical Report CMS-PAS-JME-13-006, CERN, Geneva, 2013.

[3] CMS Collaboration, "Boosted Top Jet Tagging at CMS", CMS Physics Analysis Summary CMS-PAS-JME-13-007, 2014.

[4] CMS Collaboration, "The CMS experiment at the CERN LHC", *JINST* **3** (2008) S08004, doi:10.1088/1748-0221/3/08/S08004.

[5] T. C. collaboration, "Determination of jet energy calibration and transverse momentum resolution in CMS", *Journal of Instrumentation* **6** (2011), no. 11, P11002.

[6] M. Cacciari, G. P. Salam, and G. Soyez, "The Catchment Area of Jets", *JHEP* **0804** (2008) 005, doi:10.1088/1126-6708/2008/04/005, arXiv:0802.1188.

[7] D. Krohn, J. Thaler, and L.-T. Wang, "Jet Trimming", *JHEP* **1002** (2010) 084, doi:10.1007/JHEP02(2010)084, arXiv:0912.1342.

[8] S. D. Ellis, C. K. Vermilion, and J. R. Walsh, "Recombination Algorithms and Jet Substructure: Pruning as a Tool for Heavy Particle Searches", *Phys.Rev.* **D81** (2010) 094023, doi:10.1103/PhysRevD.81.094023, arXiv:0912.0033.

[9] A. J. Larkoski, S. Marzani, G. Soyez, and J. Thaler, "Soft Drop", *JHEP* **1405** (2014) 146, doi:10.1007/JHEP05(2014)146, arXiv:1402.2657.

[10] M. Dasgupta, A. Fregoso, S. Marzani, and G. P. Salam, "Towards an understanding of jet substructure", *JHEP* **1309** (2013) 029, doi:10.1007/JHEP09(2013)029, arXiv:1307.0007.

[11] P. Berta, M. Spousta, D. W. Miller, and R. Leitner, "Particle-level pileup subtraction for jets and jet shapes", *JHEP 06 (2014) 092* (2014) arXiv:1403.3108.

[12] D. Krohn, M. Schwartz, M. Low, and L.-T. Wang, "Jet Cleansing: Pileup Removal at High Luminosity", arXiv:1309.4777v1.

[13] D. Bertolini, P. Harris, M. Low, and N. Tran, "Pileup Per Particle Identification", arXiv:1407.6013.

[14] CMS Collaboration, "Particle Flow Event Reconstruction in CMS and Performance for Jets, Taus, and MET", *CMS Physics Analysis Summary* **CMS-PAS-PFT-09-001** (2009).

[15] CMS Collaboration, "Commissioning of the Particle-flow Event Reconstruction with the first LHC collisions recorded in the CMS detector", *CMS Physics Analysis Summary* **CMS-PAS-PFT-10-001** (2010).

[16] CMS Collaboration Collaboration, "Search for heavy resonances in the W/Z-tagged dijet mass spectrum in pp collisions at 7 TeV", *Phys.Lett.* **B723** (2013) 280–301, doi:10.1016/j.physletb.2013.05.040, arXiv:1212.1910.

[17] L. Randall and R. Sundrum, "A large mass hierarchy from a small extra dimension", *Phys. Rev. Lett* **83** (1999) 3370, arXiv:hep-ph/99905221.

[18] T. Sjostrand, S. Mrenna, and P. Skands, "PYTHIA 6.4 physics and manual", *JHEP* **05** (2006) 026, doi:10.1088/1126-6708/2006/05/026, arXiv:hep-ph/0603175.

[19] R. Field, "Min-Bias and the Underlying Event at the LHC", *Acta Phys.Polon.* **B42** (2011) 2631–2656, doi:10.5506/APhysPolB.42.2631, arXiv:1110.5530.

[20] M. Bahr et al., "Herwig++ Physics and Manual", *Eur.Phys.J* **C58** (2008) 639–707, doi:10.1140/epjc/s10052-008-0798-9, arXiv:arXiv:0803.0883.

[21] T. Sjostrand, S. Mrenna, and P. Skands, "A brief introduction to PYTHIA 8.1", *Comput. Phys. Comm.* **178** (2008) 852–867, doi:10.1016/j.cpc.2008.01.036, arXiv:0710.3820.

[22] CMS Collaboration, "8 TeV Jet Energy Corrections and Uncertainties based on 19.8 fb^{-1}", CMS Detector Performance Note CMS-DP-2013-033, 2013.

[23] M. Cacciari, G. P. Salam, and G. Soyez, "The anti-k_t jet clustering algorithm", *JHEP* **04** (2008) 063, doi:10.1088/1126-6708/2008/04/063, arXiv:0802.1189.

[24] CMS Collaboration, "Photon ID performance with 19.6 fb^{-1} of data collected at $\sqrt{s} = 8$ TeV with the CMS detector", CMS Detector Performance Note CMS-DP-2013-010, 2013.

[25] CMS Collaboration, "Jet Energy Corrections for Multiple Cone Sizes", cms detector performance note in preparation, 2014.

[26] J. M. Butterworth, A. R. Davison, M. Rubin, and G. P. Salam, "Jet substructure as a new Higgs search channel at the LHC", arXiv:0810.0409.

[27] J. Thaler and K. Van Tilburg, "Identifying Boosted Objects with N-subjettiness", *JHEP* **1103** (2011) 015, doi:10.1007/JHEP03(2011)015, arXiv:1011.2268.

[28] Y. L. Dokshitzer, G. Leder, S. Moretti, and B. Webber, "Better jet clustering algorithms", *JHEP* **9708** (1997) 001, doi:10.1088/1126-6708/1997/08/001, arXiv:hep-ph/9707323.

[29] M. Cacciari, G. P. Salam, and G. Soyez, "On the use of charged-track information to subtract neutral pileup", arXiv:1404.7353.

[30] M. Cacciari and G. P. Salam, "Pileup subtraction using jet areas", *Phys.Lett.* **B659** (2008) 119–126, doi:10.1016/j.physletb.2007.09.077, arXiv:0707.1378.

[31] G. Soyez et al., "Pileup subtraction for jet shapes", *Phys.Rev.Lett.* **110** (2013), no. 16, 162001, doi:10.1103/PhysRevLett.110.162001, arXiv:1211.2811.

[32] CMS Collaboration Collaboration, "Studies of jet mass in dijet and W/Z + jet events", *JHEP* **1305** (2013) 090, doi:10.1007/JHEP05(2013)090, arXiv:1303.4811.